Spot-Size Converter Based on Long-Period Grating

Jia Yao Deng, Meng Ke Wang, Xiao Xia Ma, Hui Jun Li, Jie Yun Wu, and Kai Xin Chen, *Member, IEEE*

***Abstract*—We propose a spot-size converter (SSC) by exploiting the high-efficiency mode conversion capability that a long-period grating (LPG) possesses. Our proof-of-concept LPG-based SSC, fabricated with optical polymer material on silicon nitride (Si_3N_4) platform, has a length of ∼700 μm, can improve the coupling efficiency between the $LP^x{}_{01}$ mode of an ultra-high numerical aperture fiber and the $E^x{}_{11}$ mode of the Si_3N_4 waveguide from ∼24% to ∼33% at 1548 nm wavelength, corresponding to 1.4-dB reduction in insertion loss. Therein, the LPG achieves a maximum mode conversion efficiency of 90% between the two $E^x{}_{11}$ modes of the polymer cladding and the Si_3N_4 core. Our proposed SSC provides a new path to achieve low-loss fiber-to-chip coupling.**

***Index Terms*—Optical coupling, spot-size converter, long-period gratings, Si_3N_4 waveguide.**

I. Introduction

Thanks to the high-index-contrast material platforms, including silicon-on-insulator (SOI), silicon nitride (Si_3N_4), and lithium niobate on insulate (LNOI) and so on, enabling ultrasmall-bending-radius and low-loss optical waveguides, various advanced and high-density photonic integrated circuits have been bloomed over the past decades [1]–[5]. However, the waveguides based on the above high-index-contrast material platforms have quite small mode size usually, resulting in a large mode field mismatch and hence a large coupling loss, when butt-coupled with a standard single mode fiber [6]. This severely limits the practical applications of these photonic integrated circuits structured on the high-index-contrast waveguide platforms.

Nowadays, spot-size conversion is considered an optimal way to address the above coupling loss issue [6], and kinds of spot-size converter (SSC) have been proposed, including cantilever couplers [7], three-dimensional (3-D) tapered coupler [8], suspended tapered coupler [9], bilevel tapers [10], inverted taper [11]–[14], bilevel inverted tapers [15], [16], arrayed waveguides [17], and staircase structure [18], and so on. Among of them, inverted tapers are widely used to structure SSCs because they could achieve ultra-low coupling loss. In fact, the cantilever coupler in [7] also employs the inverted taper structure. This coupler, which combines inverted taper with cantilever, is designed for coupling light signal into/out SOI waveguide. The fabricated coupler achieves a quite low coupling loss of 0.48/0.39 dB/facet for the quasi-TE/-TM modes at 1550 nm, respectively, and less than 1 dB/facet from 1477 to 1580 nm for both polarizations, when butt-coupled with a tapered optical fiber. But its fabrication involves the complicated processes to release the cantilevers from the substrate by anisotropically etching the SiO_2 and isotropically etching the Si substrate. In addition, in [13], the fabricated inverted taper SSC for Si_3N_4 waveguide achieves coupling losses as low as 0.12 and 0.14 dB/facet at 976 and 1550 nm wavelengths, when butted-coupled with a high numerical aperture fiber (UHNA3) and a single-mode fiber (SM-1550), respectively. And the coupling losses is lower than 0.2 dB/facet in the wavelength range of 1460 to 1635 nm. In [16], the fabricated bilayer inverted taper for LNOI waveguide achieves a low coupling loss of 0.54/0.59 dB/facet at 1550 nm for the TE/TM polarization, respectively, and less than 1 dB/facet for both TE and TM polarizations in the wavelength range of 1527 to 1630 nm, when butt-coupled with an ultra-high numerical aperture fiber (UHNAF) of which the mode field diameter is about 3.2 μm. Especially, in [14], a two-inversed-taper SSC designed for the coupling between the $LP_{11a.x}$ and TE_1 modes achieves experimentally an average of 5.51 dB coupling loss in the wavelength range of 1515–1585 nm. These above SCCs help to improve the butt-coupling efficiency efficiently. However, the fabrication of them is kind of difficult due to a quite high requirement for the fabrication precision.

In this paper, we propose an SSC based on a long-period grating (LPG). As is well known, at resonance wavelengths, an LPG can couple the mode of the cladding into the mode of the core completely and vice versa [19], [20]. By exploiting this unique capability, LPG-based wavelength filter [21]–[23], mode filter [24], [25], mode switch [26], mode converter [27]–[30], grating coupler [31], and optical-fiber-to-waveguide coupler [32] have been proposed and demonstrated recent years. Note that the transfer of light power between the fiber and the waveguide in [32] is based on the grating-assisted transverse coupling, not butt coupling via the facets of the fiber and the waveguide. Similarly, this unique transverse mode coupling capability of an LPG can also be exploited to achieve the conversion between a small-size core mode and a large-size cladding mode and, hence, realize the SSC. To demonstrate this idea experimentally, we fabricated the proposed LPG-based SSC with optical polymer material on Si_3N_4 platform. Our typical fabricated SSC, which has a grating length of ∼700 μm, can improve the coupling efficiency between

Manuscript received March 3, 2022; accepted March 6, 2022. Date of publication March 9, 2022; date of current version April 4, 2022. This work was supported in part by the National Natural Science Foundation of China under Grants 62075027 and U20A20165, in part by the Key Research and Development Program of Sichuan Province under Grant 2020YFSY0003, in part by the Wuhan National Laboratory for Optoelectronics under Grant 2019WNLOKF001, and in part by the Fundamental Research Funds for the Central Universities under Grants ZYGX2019J050 and ZYGX2020ZB015. *(Corresponding author: Kai Xin Chen.)*

The authors are with the School of Optoelectronic Science and Engineering, University of Electronic Science and Technology of China, Chengdu 611731, China (e-mail: deng_jiayao@std.uestc.edu.cn; wmk@std.uestc.edu.cn; maxiaoxia_cd@163.com; ljh@std.uestc.edu.cn; jieyunwu@uestc.edu.cn; chenkx@uestc.edu.cn).

Digital Object Identifier 10.1109/JPHOT.2022.3157946

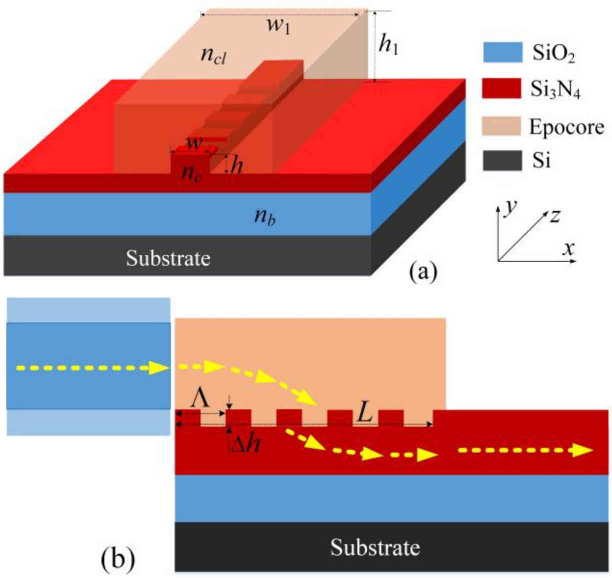

Fig. 1. Schematic diagram showing (a) the structure and (b) the operation principle of the proposed LPG-based SSC.

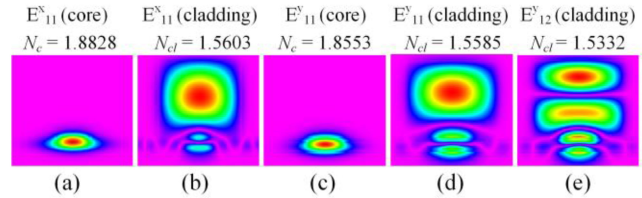

Fig. 2. Effective refractive indices and intensity patterns of the involved (a), (c) core and (b), (d), (e) cladding modes.

the $LP^x{}_{01}$ mode of an UHNAF and the $E^x{}_{11}$ mode of the Si_3N_4 rib waveguide from ~24% to ~33% at 1548 nm wavelength, corresponding to 1.4-dB reduction in insertion loss. Therein, the LPG achieves a maximum mode conversion efficiency of 90% between the two $E^x{}_{11}$ modes of the polymer cladding and the Si_3N_4 core. The 3-dB bandwidth of the device is 4 nm, but it can be dramatically enlarged by optimizing the design of the grating, such as by using the chirped grating [33] or the length-apodized grating [25], [29], or by operating an LPG at its turning point along its phase-matching curve [30], [34].

II. Configuration and Design

Fig. 1(a) shows schematically the proposed LPG-based SSC, which consists of a corrugated LPG formed on the ridge of a Si_3N_4 rib waveguide and covered with a channel-shaped cladding formed with polymer Epocore. The thickness of the Si_3N_4 film is 0.9 μm, formed on a silica buffer layer. The thickness and the width of the channel-shaped polymer cladding are h_1 and w_1, respectively. The Si_3N_4 rib waveguide has a ridge width w and a height h (i.e., the etching depth). The corrugated LPG has a period Λ, an etching depth Δh, and a length L, as shown in Fig. 1(b). The refractive indices of the core (Si_3N_4), the cladding (Epocore), and the buffer (SiO_2) are denoted as n_c, n_{cl}, and n_b, respectively, and $n_c = 1.9963$, $n_{cl} = 1.5716$, and $n_b = 1.4440$ at 1550 nm wavelength for both TE and TM polarizations. The operation principle of the proposed SSC is also shown schematically in Fig. 1(b). The light signal from the input fiber is butt-coupled into the channel-shaped polymer cladding and then coupled into the Si_3N_4 core via the LPG when it propagates along the channel-shaped cladding. Similarly, the output signal experiences the inverted path and is butt-coupled into the output fiber.

The butt-coupling efficiency η between the modes of the fiber and the cladding can be expressed as [35]:

$$\eta = \frac{\int (\vec{E}_f \times \vec{H}_c^* \cdot d\vec{S}) \int (\vec{E}_c \times \vec{H}_f^* \cdot d\vec{S})}{\int (\vec{E}_f \times \vec{H}_f^* \cdot d\vec{S}) \mathrm{Re} \int (\vec{E}_c \times \vec{H}_c^* \cdot d\vec{S})} \quad (1)$$

where E_f, H_f, E_c, and H_c represent the normalized electric (E) and magnetic (H) fields of the modes in the fiber (subscript f) and the cladding (subscript c), respectively. The values of these fields can be obtained with a commercial model solver (COMSOL). For the convenience of measurement and comparison, in this work an UHNAF with a mode-field diameter of 4.3 μm at 1550 nm wavelength is used to butt-couple the LP_{01} mode into the Epocore cladding or the Si_3N_4 core. To match the mode field of the UHNAF as soon as possible, both the width w_1 and thickness h_1 of the Epocore cladding are calculated to be 5.0 μm. Meanwhile, the ridge width w and height h of the Si_3N_4 rib waveguide are set to 2.0 μm and 0.3 μm, respectively. With these parameters, the η between the $LP^x{}_{01}$ mode of the UHNAF and the $E^x{}_{11}$ mode of the Epocore cladding is calculated to be 91.9%. However, the calculated η between the same fiber mode and the $E^x{}_{11}$ mode of the Si_3N_4 core is only 39.8%.

As aforementioned, the light signal launched into the Epocore cladding needs to be coupled efficiently into the Si_3N_4 core via the LPG. Apart from the waveguide parameters, the performances of an LPG are determined by its period Λ, etching depth Δh, and length L, in which the period Λ is given by [20]:

$$\Lambda = \frac{\lambda_0}{(N_c - N_{cl})} \quad (2)$$

where N_c and N_{cl} are the effective indices of the two coupled core and cladding modes, respectively, λ_0 is the resonant wavelength of the LPG. Using above Si_3N_4 core and Epocore cladding parameters, the intensity patterns and the effective refractive indices of the supermodes of the entire structure are calculated at 1550 nm wavelength with a commercial model solver (Rsoft). Here we differentiate the cladding and the core modes according to their respective strongest mode field pattern and then label them according to usual rules. The results are shown in Figs 2(a)-(e), respectively. With these index values, the calculated Λ for the coupling between the two $E^x{}_{11}$ modes is ~4.81 μm, while for the coupling between the two $E^y{}_{11}$ modes is ~5.22 μm. Note that the calculated Λ for the coupling between the $E^y{}_{11}$ mode of the core and the $E^y{}_{12}$ mode of the cladding is also ~4.81 μm. These results indicate that, at 1550 nm wavelength, the designed LPG with $\Lambda = 4.81$ μm can achieve the coupling not only between the two $E^x{}_{11}$ modes of the core and the cladding,

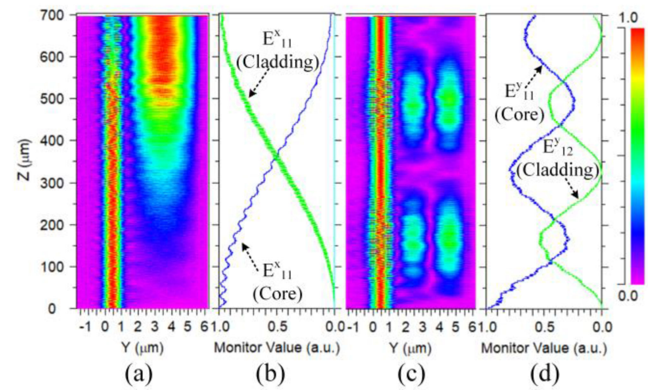

Fig. 3. (a), (c) Propagation dynamics and (b), (d) normalized power of the monitored modes along the coupling region of the proposed LPG-based SSC when (a), (b) the $E^x{}_{11}$ and (c), (d) $E^y{}_{11}$ modes at 1550 nm are launched into the Si_3N_4 core.

TABLE I
DESIGNED AND MEASURED MORPHOLOGICAL PARAMETERS OF THE FABRICATED DEVICE

Parameters	Optimized design	Measured value
w (μm)	2.0	2.7
w_1 (μm)	5.0	5.2
h_1 (μm)	5.0	5.2
h (μm)	0.3	0.3
Δh (nm)	60	57
Λ (μm)	4.8	4.7
Duty cycle	0.5	0.55

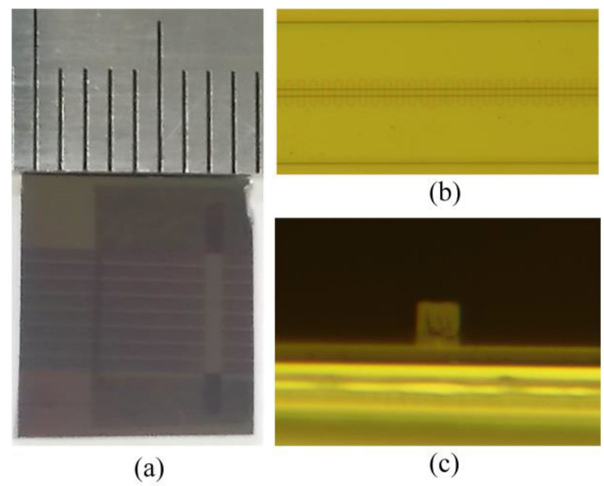

Fig. 4. (a) Photograph of the fabricated device, (b) microscopic image of partial grating after ICP etching but before coating Epocore cladding, and (c) microscopic image of the end face of the device.

but also between the $E^y{}_{11}$ mode of the core and the $E^y{}_{12}$ mode of the cladding. However, it cannot achieve the coupling between the two $E^y{}_{11}$ modes of the core and the cladding at this wavelength. Although the materials used in this work have negligible birefringence, the asymmetric waveguide and device structure result in different grating periods for the two polarizations. In view of this, the proposed LPG-based SSC is optimized only for the TE polarization.

The coupling lengths L of the grating is calculated by simulation of light propagation along the designed LPG with a three-dimensional finite-difference beam propagation method (3DFD-BPM) (BeamPROP, RSoft), and the period is further optimized in this simulation process. To minimize the scattering losses caused by the grating, here the grating depth Δh and the duty cycle of the grating are set to 0.06 μm and 0.5. The calculated L is 700 μm and the period Λ is further optimized to be 4.87 μm for the coupling between the two $E^x{}_{11}$ modes of the core and the cladding. In Fig. 3(a)-(d), we present the simulated propagation and the normalized power of the monitored modes along the coupling region of the proposed SSC when the $E^x{}_{11}$ and $E^y{}_{11}$ mode at 1550 nm are launched into the Si_3N_4 core, respectively. From Fig. 3(a) and (b), the launched $E^x{}_{11}$ mode can couple almost completely to the $E^x{}_{11}$ modes of the cladding at $L = 700$ μm. However, from Fig. 3(c) and (d), the launched $E^y{}_{11}$ mode will couple partially ($\sim$55%) to the $E^y{}_{12}$ modes of the cladding at $L = 325$ μm, as expected.

III. FABRICATION AND CHARACTERIZATION

With the designed device parameters, we fabricated the proposed LPG-based SSC by the standard photolithography and the dry etching techniques. The Si_3N_4 thin film sample, which consists of a layer of 900-nm thick Si_3N_4 thin film deposited on the surface of a 3-μm thick silica layer formed on a 500-μm thick silicon substrate, was used to fabricate the proposed device. The fabrication processes are described briefly below. Firstly, a layer of $\sim$ 200-nm thick chromium (Cr) film was deposited on the Si_3N_4 film by radio-frequency magnetron sputtering. Secondly, the photoresist pattern of the designed straight channel waveguides was formed by standard photolithography and then transferred to the Cr film by chemical etching. Thirdly, the designed Si_3N_4 rib waveguides were realized by inductively coupled plasma (ICP) etching with the mixture gases of Ar and CF_4. Next, the grating structure was formed on the ridge by the photolithography and ICP processes. Subsequently, a 5-μm thick Epocore cladding was spin-coated on the simple and chemically etched into the rectangular channel around the Si_3N_4 core by the photolithography process. Finally, the silicon substrate of the sample was cleaved to form input/output facet. To avoid damaging the grating, we have to retain a section of Si_3N_4 core without grating when cleaving the sample, which will increase slightly the length ($\sim$2 mm) and the propagation loss of the device. In this work, we fabricated a set of identical Si_3N_4 rib waveguides in the same sample, but the LPGs and corresponding Epocore cladding channels were formed only on part of them and only one end of the sample. Thus, by comparing the differences of the insertion losses of the waveguides with and without LPG, the performances of the proposed SSC can be easily obtained. Table I shows the measured morphological parameters of the fabricated device. Figs. 4(a), (b), and (c) show, respectively, a photograph of the fabricated device, a microscopic image of partial grating after ICP etching but before coating Epocore

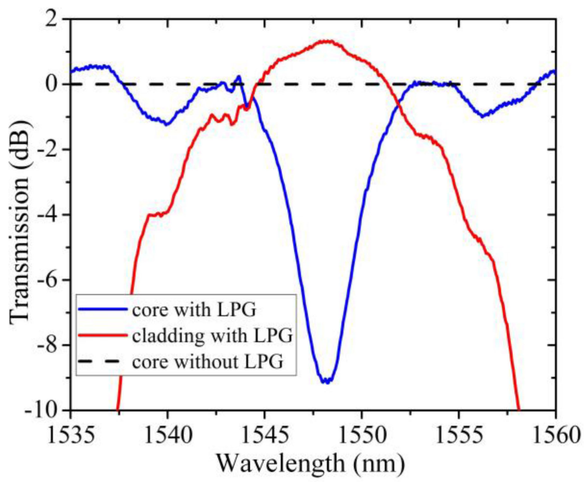

Fig. 5. Normalized transmission spectra of the $E^x{}_{11}$ mode when the $LP^x{}_{01}$ mode from an ASE light source was launched into the cladding, the core, both with the LPG, and the core without the LPG via the UHNAF.

cladding, and a microscopic image of the end face of the device. In Fig. 4(c), we can dimly see the Si_3N_4 waveguide core.

To characterize the fabricated LPG-based SSC, we launched the output light from an amplified spontaneous emission (ASE) light source (B&A, AS4600) into the Epocore cladding, the Si_3N_4 core with LPG, and the Si_3N_4 core without LPG, respectively, via an UHNAF with a mode field diameter of $\sim$4.3 μm. Considering that for the first two cases, it is very possible to excite the core $E^x{}_{11}$ mode and the cladding $E^x{}_{11}$ mode (even higher-order modes in the cladding) simultaneously. Thus, to excite the unwanted modes as little as possible, the position of the fiber was adjusted carefully to launch the light signal exactly at the center of the Epocore cladding and the Si_3N_4 core. It should be pointed out here that these excited unwanted modes have a quite slight impact on the evaluation of the butt-coupling efficiency. But their impact on the application of the proposed SSC is negligible. We chose only the TE polarization input with an optical fiber online polarizer and a polarization controller placed along the input UHNAF. The light from the output Si_3N_4 cores were collected by another UHNAF and monitored by an optical spectrum analyzer (OSA) (Anristu MS97740A).

The measured transmission spectra of the excited $E^x{}_{11}$ mode when launching the light signal into the Epocore cladding, the Si_3N_4 core with and without the LPG are normalized with respect to that of the last case, respectively, and results are shown in Fig. 5. It can be seen that compared with the transmission via the Si_3N_4 core without the LPG, the transmission via the polymer cladding and the LPG increases 1.4 dB at 1548 nm wavelength. Meanwhile, by comparing the transmission spectra via the Si_3N_4 core with the LPG at different wavelengths, we can deduce that the fabricated LPG achieve a mode conversion efficiency of 90% (corresponding to 0.46-dB coupling loss) at 1548 nm wavelength. Further, the measured insertion losses when launching the light signal into the Epocore cladding and the Si_3N_4 core without the LPG are $\sim$11 dB and $\sim$12.4 dB, respectively. If we ignore the transmission losses of the Si_3N_4 core and the Epocore cladding, then the coupling loss between the UHNAF and the Si_3N_4 core without the LPG is 6.2 dB/facet (the two facets are considered to be the same completely), corresponding to a coupling efficiency of $\sim$24%. Next, according to the coupling loss (0.46 dB) of the LPG and another insertion loss (11 dB), we can get that the coupling loss between the UHNAF and the Epocore cladding is 4.34 dB, corresponding to a coupling efficiency of $\sim$36.8%. Thus, according to the above results, we can deduce that our fabricated SSC can improve the coupling efficiency between the $LP^x{}_{01}$ mode of the UHNAF and the $E^x{}_{11}$ mode of the Si_3N_4 waveguide from $\sim$24% to $\sim$33% at 1548 nm wavelength. The improvement of the coupling efficiency is not large enough. This can be mainly attributed to a quite large coupling loss of 4.34 dB between the UHNAF and the Epocore cladding, caused mainly by the imperfect facet obtained by cleaving silicon substrate. Additionally, a somewhat large fabrication error is another factor caused this large coupling loss issue. We believe there should be much room to improve the performances of our device by improving the quality of the facet and the fabrication skill. In considering that the polymer is hard to polish, thus improving the quality of the facet is mainly by improving cleaving skill. However, if we use inorganic silicon oxynitride to replace the polymer Epocore, then the quality of the facet can be improved remarkably by polishing it. In addition, as a conventional LPG used in this work is a strongly wavelength-selective device [19], the 3-dB bandwidth of the device is only 4 nm, but it can be dramatically enlarged by the method introduced in the introduction section.

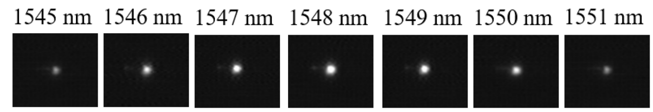

Fig. 6. Output near-field patterns taken with an infrared camera at different wavelengths.

To further confirm that the fabricated LPG achieves the mode conversion between the core and the cladding, we launched the $LP^x{}_{01}$ mode from a tunable laser (Santur TL-2020-C-107) into the polymer cladding with the LPG via the UHNAF and took the output near-field pattern from the Si_3N_4 core with an infrared camera (Micron Viewer 7290A) around the rejection band. The results are shown in Fig. 6. It can be seen the largest output power corresponds to 1548 nm, i.e., the resonance wavelength shown in Fig. 5, while the output power becomes weak at these off-resonance wavelengths. These results confirm the light propagation process is related to the mode conversion between the core and the cladding.

V. Conclusion

We have proposed and demonstrated an LPG-based SSC. Our proof-of-concept SSC, fabricated with optical polymer material on Si_3N_4 platform, can improve the butt-coupling efficiency between the UHNAF and the Si_3N_4 waveguide from $\sim$24% to $\sim$33% at 1548 nm wavelength. The 3-dB bandwidth of the device is 4 nm. Compared with these previously reported SSCs, our proposed SSC has the advantages of simple structure and easy fabrication. It is feasible with inexpensive i-line lithography and could also be realized with other materials platforms.

REFERENCES

[1] R. Soref, "The past, present, and future of silicon photonics," *IEEE J. Sel. Top. Quantum Electron.*, vol. 12, no. 6, pp. 1678–1687, Nov./Dec. 2006.

[2] S. Han, T. J. Seok, N. Quack, B. W. Yoo, and M. C. Wu, "Large-scale silicon photonic switches with movable directional couplers," *Optica*, vol. 2, no. 4, pp. 370–375, Apr. 2015.

[3] J. C. Adcock *et al.*, "Advances in silicon quantum photonics," *IEEE J. Sel. Top. Quantum Electron.*, vol. 27, no. 2, pp. 1–24, Mar./Apr. 2021.

[4] R. Moreira, S. Gundavarapu, and D. J. Blumenthal, "Programmable eye-opener lattice filter for multi-channel dispersion compensation using an integrated compact low-loss silicon nitride platform," *Opt. Exp.*, vol. 24, no. 15, pp. 16732–16742, Jul. 2016.

[5] D. Zhu *et al.*, "Integrated photonics on thin-film lithium niobate," *Adv. Opt. Photon.*, vol. 13, no. 2, pp. 242–352, Jun. 2021.

[6] R. Marchetti, C. Lacava, L. Carroll, K. Gradkowski, and P. Minzioni, "Coupling strategies for silicon photonics integrated chips," *Photon. Res.*, vol. 7, no. 2, pp. 201–239, Feb. 2019.

[7] M. Wood, P. Sun, and R. M. Reano, "Compact cantilever couplers for low-loss fiber coupling to silicon photonic integrated circuits," *Opt. Exp.*, vol. 20, no. 1, pp. 164–172, Jan. 2012.

[8] C. W. Liao, Y. T. Yang, S. W. Huang, and M. C. M. Lee, "Fiber-core-matched three-dimensional adiabatic tapered couplers for integrated photonic devices," *J. Lightw. Technol.*, vol. 29, no. 5, pp. 770–774, Mar. 2011.

[9] Q. Fang *et al.*, "Suspended optical fiber-to-waveguide mode size converter for silicon photonics," *Opt. Exp.*, vol. 18, no. 8, pp. 7763–7769, Apr. 2010.

[10] D. Dai, S. He, and H. K. Tsang, "Bilevel mode converter between a silicon nanowire waveguide and a larger waveguide," *J. Lightw. Technol.*, vol. 24, no. 6, pp. 2428–2433, Jun. 2006.

[11] N. Lindenmann, G. Balthasar, D. Hillerkuss, R. Schmogrow, and C. Koos, "Photonic wire bonding: A novel concept for chip-scale interconnects," *Opt. Exp.*, vol. 20, no. 16, pp. 17667–17677, Jul. 2012.

[12] T. C. Zhu, Y. W. Hu, P. Gatkine, S. Veilleux, J. Bland-Hawthorn, and M. Dagenaiset, "Ultrabroadband high coupling efficiency fiber-to-waveguide coupler using Si_3N_4/SiO_2 waveguides on Silicon," *IEEE Photon. J.*, vol. 8, no. 5, Oct. 2016, Art. no. 7102112.

[13] J. F. Mu *et al.*, "Low-loss, broadband and high fabrication tolerant vertically tapered optical couplers for monolithic integration of Si_3N_4 and polymer waveguides," *Opt. Lett.*, vol. 42, no. 19, pp. 3812–3815, Oct. 2017.

[14] Y. X. Lai, Y. Yu, S. Q. Fu, J. Xu, P. P. Shum, and X. L. Zhang, "Efficient spot size converter for higher-order mode fiber-chip coupling," *Opt. Lett.*, vol. 42, no. 18, pp. 3702–3705, Sep. 2017.

[15] L. Y. He, M. Zhang, A. Shams-Ansari, R. R. Zhu, C. Wang, and L. Marko, "Low-loss fiber-to-chip interface for lithium niobate photonic integrated circuits," *Opt. Lett.*, vol. 44, no. 9, pp. 2314–2317, May 2019.

[16] C. R. Hu *et al.*, "High-efficient coupler for thin-film lithium niobite waveguide devices," *Opt. Exp.*, vol. 29, no. 4, pp. 5397–5406, Feb. 2021.

[17] W. X. Liu, J. H. Zhang, L. Liu, D. X. Dai, and Y. C. Shi, "High efficiency silicon edge coupler based on uniform arrayed waveguides with un-patterned cladding," *IEEE Photon. Technol. Lett.*, vol. 32, no. 17, pp. 1077–1080, Sep. 2020.

[18] M. K. Wang, J. H. Li, H. Yao, Y. J. Long, F. Zhang, and K. X. Chen, "A cost-effective edge coupler with high polarization selectivity for thin film lithium niobate modulators," *IEEE J. Lightw. Technol.*, vol. 40, no. 4, pp. 1105–1111, Feb. 2022.

[19] A. M. Vengsarkar, P. J. Lemaire, J. B. Judkins, V. Bhatia, T. Erdogan, and E J. Sipe, "Long-period fiber grating as band-rejection filters," *IEEE J. Lightw. Technol.*, vol. 14, no. 1, pp. 58–65, Jan. 1996.

[20] V. Rastogi and K. S. Chiang, "Long-period gratings in planar optical waveguides," *Appl. Opt.*, vol. 41, no. 30, pp. 6351–6355, Oct. 2002.

[21] M. S. Kwon and S. Y. Shin, "Characteristics of polymer waveguide notch filters using thermooptic long-period gratings," *IEEE J. Sel. Top. Quantum Electron.*, vol. 11, no. 1, pp. 190–196, Jan./Feb. 2005.

[22] W. Jin, K. S. Chiang, and Q. Liu, "Thermally tunable lithium-niobate long-period waveguide grating filter fabricated by reactive ion etching," *Opt. Lett.*, vol. 35, no. 4, pp. 484–486, Feb. 2010.

[23] Y. B. Cho, B. K. Yang, J. H. Lee, J. B. Yoon, and S. Y. Shin, "Silicon photonic wire filter using asymmetric sidewall long-period waveguide grating in a two-mode waveguide," *IEEE Photon. Technol. Lett.*, vol. 20, no. 7, pp. 520–522, Apr. 2008.

[24] J. H. Li, M. H. Zhou, H. Yao, M. K. Wang, J. Y. Wu, and K. X. Chen, "Grating-assisted directional coupler in lithium niobate for tunable mode filtering," *IEEE Photon. J.*, vol. 13, no. 2, Apr. 2021, Art. no. 6600807.

[25] Q. D. Huang, W. Wang, W. Jin, and K. S. Chiang, "Ultra-broadband mode filter based on phase-shifted long-period grating," *IEEE Photon. Technol. Lett.*, vol. 31, no. 13, pp. 1052–1055, Jul. 2019.

[26] W. Jin and K. S. Chiang, "Mode switch based on electro-optic long-period waveguide grating in lithium niobate," *Opt. Lett.*, vol. 40, no. 2, pp. 237–240, Jan. 2015.

[27] Y. Yang, K. X. Chen, W. Jin, and K. S. Chiang, "Widely wavelength-tunable mode converter based on polymer waveguide grating," *IEEE Photon. Technol. Lett.*, vol. 27, no. 18, pp. 1985–1988, Sep. 2015.

[28] W. Jin and K. S. Chiang, "Three-dimensional long-period waveguide gratings for mode-division-multiplexing applications," *Opt. Exp.*, vol. 26, no. 12, pp. 15289–15299, Jun. 2018.

[29] W. Wang, J. Y. Wang, K. X. Chen, W. Jin, and K. S. Chiang, "Ultra-broadband mode converters based on length-apodized long-period waveguide gratings," *Opt. Exp.*, vol. 25, no. 13, pp. 14341–14350, Jun. 2017.

[30] W. K. Zhao, K. X. Chen, and J. Y. Wu, "Ultra-short embedded long-period waveguide grating for broadband mode conversion," *Appl. Phys. B*, vol. 125, no. 9, pp. 1–7, Sep. 2019.

[31] Y. Bai, Q. Liu, K. P. Lor, and K. S. Chiang, "Widely tunable long-period waveguide grating couplers," *Opt. Exp.*, vol. 14, no. 26, pp. 12644–12654, Dec. 2007.

[32] B. L. Bachim, O. O. Ogunsola, and T. K. Gaylord, "Optical-fiber-to-waveguide coupling using carbon-dioxide-laser-induced long-period fiber gratings," *Opt. Lett.*, vol. 30, no. 16, pp. 2080–2082, Aug. 2005.

[33] Q. Liu and K. S. Chiang, "Design of long-period waveguide grating filter by control of waveguide cladding profile," *J. Lightw. Technol.*, vol. 24, no. 9, pp. 3540–3546, Sep. 2006.

[34] W. Jin and K. S. Chiang, "Leaky-mode long-period grating on a lithium-niobate-on-insulator waveguide," *Optica*, vol. 8, no. 12, pp. 1624–1631, Dec. 2021.

[35] K. Okamoto, *Fundamentals of Optical Waveguides*. Burlington, MA, USA: Elsevier, 2006, pp. 159–162.